analytical chemistry

ARTICLE

pubs.acs.org/ac

A Device for Gated Autosynchronous Luminescence Detection

Russell Connally*

Macquarie University, Balaclava Road, North Ryde Sydney, NSW, 2109, Australia

Supporting Information

ABSTRACT: The sensitive detection of delayed luminescence ($\tau > 100\ \mu s$) can be achieved with an optomechanical instrument, the gated autosynchronous luminescence detector (GALD). The device effectively combines an excitation chopper, a detection chopper, and a dichroic mirror into a single element. With dimensions of 12 mm (H), 32 mm (W), and 90 mm (L), it is designed for insertion into the differential interference contrast (DIC) prism slot of a BX51 Olympus microscope. The GALD described here employed a compact high-power UV LED as the excitation source to capture images of *Giardia lamblia* cysts indirectly labeled with a europium chelate/streptavidin conjugate. Labeled cells were clearly visible in the complete absence of autofluorescence and signal intensity was sufficient to capture high-resolution color images within several seconds. Shorter exposure intervals of 100 ms on a monochrome Andor iXON camera delivered time-gated luminescence images with a signal-to-noise ratio better than 114:1.

Luminescence is the emission of light arising from an electronically excited state; it is formally categorized as either fluorescence or phosphorescence depending on the nature of the excited state. When the electron in the excited state is paired by a ground state electron of opposite spin, photon emission is characterized by a short lifetime (~10 ns) and is termed fluorescence. Conversely, when photon emission arises from relaxation of an electron from the triplet excited state, where both ground state and excited state electrons share the same spin, transitions are forbidden and lifetimes are typically milliseconds to seconds.[1] Interestingly, lanthanides show delayed fluorescence in which the triplet state is temporarily involved, but transition is from the first excited state. Luminescence lifetimes of hundreds of microseconds to milliseconds are observed for europium and terbium trivalent ions. Lanthanide ions have a low absorbance cross-section, and luminescence output is enhanced by chelation of the ions with a sensitizer molecule. Excitation of the attached ion occurs through a chain of events; the sensitizer molecule is excited to the singlet state from which it decays via intersystem crossing and other processes to the triplet state whereon energy transfer occurs to the chelated ion via metal ligand bonds. Crucially, triplet state energy levels of the sensitizer must sit sufficiently above the receiving state of the lanthanide ion to ensure that back transfer via phonon interactions cannot easily occur.

Fluorescence microscopy is a valuable technique that can deliver a huge increase in the ability to detect signals of interest compared with bright-field illumination. Conventionally, the object of interest is labeled with a fluorescent dye and observed through the fluorescence microscope using spectral filters to isolate the desired fluorescence signal. In some cases, the target is embedded in a matrix of intrinsically fluorescent components (autofluorophores) that acts to obscure detection due to the broad spread of the autofluorescence. Spectral selection with optical filters is not useful in these circumstances, and as a consequence, target detection becomes arduous. Examples of this include the detection of waterborne pathogens *Giardia*/*Cryptosporidium* in the particulate mass collected from large volumes of water; analysis of activated sludge and tissue samples that have been treated with formaldehyde.[2−4]

For detection of rare targets in autofluorescent environments, however, time-gated luminescence (TGL) detection greatly surmounts the capability of conventional fluorescence microscopy. More specifically, the detection of *Mycobacterium tuberculosis* in respiratory samples is a particularly challenging task; the organism is very small and the samples are strongly autofluorescent.[5,6] This application is one that would benefit greatly from a technique that reduces background autofluorescence. Time-gated luminescence (TGL) techniques rely upon the use of luminophores with lifetimes thousands of times longer (~0.1 to 2 ms) than those of prompt fluorescent dyes (~20 ns). Regimes to exploit TGL for the suppression of background autofluorescence rely upon a brief, intense pulse of light to excite both prompt and delayed luminescence from the sample. Capture of the radiant emission is delayed for a short period ($1-100\ \mu s$) to permit prompt fluorescence to decay below the detection threshold. Persistent emission from long-lived luminophores is then captured in the absence of autofluorescence by gating the detector after the resolving period; the principle is shown schematically in Figure 1. Time gated luminescence (TGL) and time-resolved fluorescence (TRF) microscopies are similar in many respects: both exploit differences in fluorescence lifetime to detect the object of interest, but they operate in different time regimes.

Received: February 1, 2011
Accepted: May 9, 2011
Published: May 09, 2011

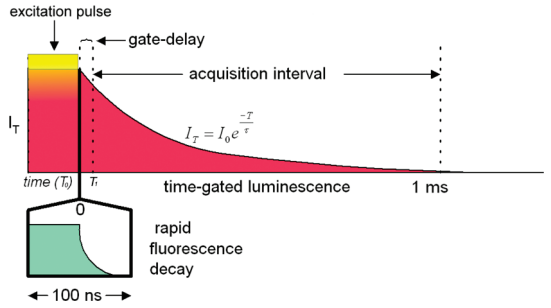

Figure 1. Time-gated luminescence detection is depicted above with time on the *X*-axis and intensity of target luminescence in arbitrary units on the *Y*-axis. The yellow region in the illustration corresponds to the application of a pulse of light (usually UV) directed on the target to excite fluorescence. At the moment excitation ceases, short-lived fluorescence (<100 ns) rapidly decays to zero as shown in the (green) enlarged view of the time-scale. The 'gate-delay' follows the excitation period and is typically a few microseconds (2−5 μs) to permit fluorescence to decay beyond detection. Luminescence from lanthanide chelates persists for many hundreds of microseconds and is easily resolved from prompt fluorescence.

While no commercial instruments are available, the mechanisms employed to construct TGL microscopes continue to evolve. The conventional means of implementing TGL microscopy in the lab rely upon the conversion of an epifluorescence microscope through the addition of a sensitive gated camera and a pulsed excitation source.[7−15] Chopper wheels are often employed to interrupt the beam from a mercury arc lamp to provide pulsed excitation.[16] Other instruments have relied upon the use of high intensity ultraviolet light-emitting diodes (UV-LEDs) because they offer very rapid transitions between the on and off state.[17] Lab-built TGL microscopes have been demonstrated to provide excellent suppression of autofluorescence.[16,18]

Cycle States in TGL Microscopy. The principle of operation for a TGL microscope is conveniently illustrated by reference to Figure 2 that shows two mechanical choppers synchronized by an external phase-locked loop (PLL) circuit. In operation, the focused beam from a continuous wave light source is interrupted by the excitation chopper wheel to generate a pulse stream. The light pulses are reflected by the dichroic mirror (within the filter cube) into the objective and focused onto the sample. The emission chopper wheel is synchronized by the PLL to block light from reaching the observer's eye during the excitation phase, but is open during the detection phase. Delayed luminescence emitted from the sample is propagated back through the objective, passing through the dichroic mirror, past the emission chopper blades, and into the eyepiece. When the choppers are operated at a sufficiently high rotation speed, long-lived luminescence is visible in the complete absence of prompt autofluorescence. The dichroic mirror is an essential component of TGL microscopes, and each mirror is designed to transmit and reflect specific wavelengths suited to the application. Europium chelates are often employed as luminescent labels due to their long lifetimes (200−700 μs) and high brightness; dichroic mirrors for this application reflect in the UV (350−400 nm) and transmit in the red (600−630 nm).

For all TGL instruments, it is necessary to precisely synchronize the excitation pulse, the resolving period, and the detection phase. The GALD inherently synchronizes these different phases to deliver a train of light pulses from pulsed or continuous wave

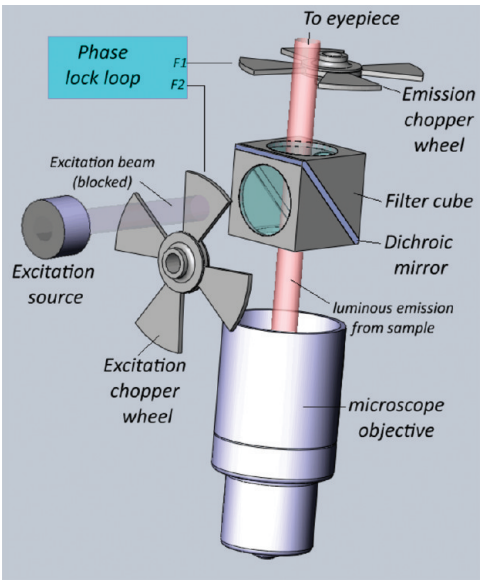

Figure 2. Early instruments designed for delayed (time-gated) luminescence microscopy employed a pair of optical choppers configured as shown here.[8,30] A phase-locked loop (PLL) is used to electronically lock the choppers and ensure that only one optical pathway (excitation or detection) is open at any time. A number of systems have also been described that use a pulsed excitation source with a chopper in the emission pathway.[7,9−11,13−15] Chopper rotation speeds vary but are typically around 6000 rpm and impose a minimum 'gate-delay' of 200−260 μs.

(CW) sources. The much wider variety of CW sources is advantageous because it is possible to increase the probe repertoire for multiparameter analyses. In this paper, I report for the first time, details of the construction of a UV LED excited GALD and applications for its use.

EXPERIMENTAL SECTION

Design of the Gated Autosynchronous Luminescence Detector (GALD). The above description of a TGL system employing mechanical shutters provides a convenient reference to compare with a compact design that performs the functions of the excitation/emission choppers and the dichroic mirror in a single assembly. Figure 3 illustrates the main features of the GALD with the upper housing and drive coils removed for the sake of clarity. The aluminum rotor face is highly polished with a mirror finish and lies at an angle of 45° to the rotor axis. The rotor may be fabricated with two blades or more; the design shown here employed dual blades with a radial sweep at the perimeter of 90°. To drive the rotor, button magnets of high coercivity are distributed in alternating polarity around the axis of the rotor. When assembled in position, the poles of the magnets lie in close proximity to a pair of electromagnet drive coils mounted on the top plate. Also mounted on the top plate is a Hall effect sensor to determine the position and polarity of the magnets as they rotate below the coils; the sensor electronics (not shown) are used to control timing and polarity of the pulses applied to the field coils.

The lightweight aluminum rotor is 29 mm in diameter and rotates at 18 500 rpm when driven with a modest 2 W of power (12 V @ 165 mA). Adjacent to the rotor is the optical excitation source, a high power ultraviolet LED (NC U033A from Nichia Corp. Japan) mounted in a low profile mount. The UV beam was focused to a

dx.doi.org/10.1021/ac200281h |*Anal. Chem.* 2011, 83, 4782–4787

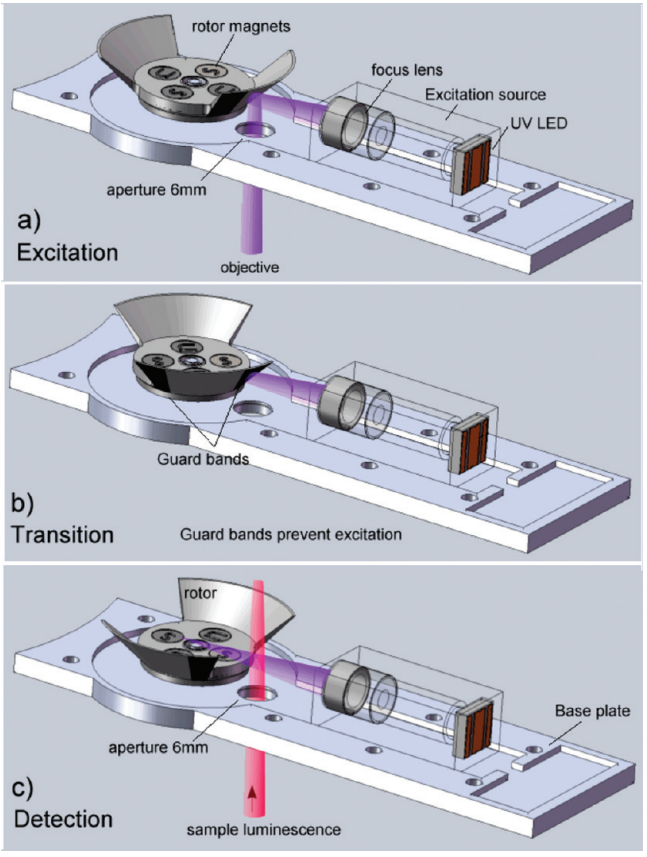

Figure 3. The component parts of the GALD are illustrated here, with the exception of the electromagnetic drive coils that sit above the rotor in the upper housing and which are hidden for the sake of clarity. The GALD is inserted into the DIC prism slot rotor so that the 6 mm aperture aligns with the optical axis of the objective. The rotor is driven electromagnetically at high speed (18 500 rpm) and a focused beam of light from an excitation source is directed onto the rotor face. The source could be a flexible *Lumatec* liquid light guide, or the UV LED assembly as shown here; the LED may be operated in continuous mode or pulsed for higher UV flux intensities. Frame 3a shows the rotor in position for the excitation cycle; collimated UV is reflected from the mirror surface of the rotor through the objective to focus on the sample. Fluorescence emission from the sample cannot propagate past the rotor blade during the excitation phase. In Figure 3b, the trailing edge of the rotor blade is now traversing the aperture; nonreflective guard bands absorb the incident excitation beam without scatter and prevent excitation of the sample. Although partially obscured by the blade, sample emission is present during this time (not shown) and visible to the observer. Figure 3c illustrates the detection phase in the TGL cycle; the rotor blades are clear of the aperture and delayed luminescence is visible to the observer. The excitation beam is absorbed on the blackened walls of the GALD housing, only the rotor face is reflective; all other surfaces are matte-black.

1 mm spot size on the rotor face using a 5.5 mm diameter lens with a focal length of 11 mm (A220, Thor Laboratories, Newton, NJ).

Guard Bands. Guard bands are nonreflective regions on the leading and trailing edges of the rotor blade. If the UV LED is actively gated, it is possible to dispense with the guard regions and ensure that the LED is only active when the aperture is completely shielded from the observer. The results presented here were gathered using electronic gating of the LED. To prevent loss of signal-to-noise ratio (SNR) when a continuous wave (CW) excitation source is employed, guard bands are used to absorb the incident beam and limit excitation of the sample to when the aperture is fully closed.

GALD States. The different TGL phases of operation are shown sequentially for the GALD in Figure 3. Excitation of the sample is shown at Figure 3a with the rotor face reflecting the excitation beam through the aperture and onto the slide carrying the sample. The *excitation* phase ends when the guard bands rotate into position. The GALD is now in the transition zone shown in Figure 3b (this corresponds to the OFF time for the LED), and excitation ceases while the trailing edge of the rotor blade transits the aperture. During this phase, the aperture is progressively opened to the observer's eye until it is fully open in the detection phase as shown in Figure 3c. Typically the transition period is complete in 260 μs, and the detection period occupies a further 810 μs. As the blade continues to rotate and partially obscure the aperture, the GALD again enters the transition zone prior to repeating the cycle. The rotation speed is high; radial velocity of the blade at the aperture center (12 mm radius, 18 500 rpm) is 23.2 $m \cdot s^{-1}$.

Typical Sensitizer Molecules. An excellent review of lanthanide sensitizers has recently been published by Bunzli.[19−22] For the work presented here, we used a derivative of BHHCT-Eu^{3+} (cat. no. 59752; Sigma-Aldrich, St. Louis, MO).[23] In the presence of a fluorescence-enhancing buffer such as that described by Arnaud,[24] these intensely luminescent chelates display a quantum yield of around 0.27 (personal communication from Prof. Jingli Yuan) and are easily coupled to immunoglobulins.

Imaging. For high speed imaging, the BX51 microscope was equipped with an Andor iXON electron amplifying CCD camera (DU-885K-C00). This (−80 °C) cooled camera supports SVGA resolution (1024 × 1024) and delivers exceptional sensitivity to enable the image-capture of labeled cysts with a single exposure of 5 ms. The color images were captured on an Olympus 12.8 megapixel DP72 camera with a sensor resolution of 4140 × 3096. This cooled camera affords high sensitivity with typical exposure intervals ranging from 10 to 100 ms.

Spectral versus Temporal Filtering. Environmentally sourced samples for fluorescence microscopy are frequently observed to contain a variety of intrinsically fluorescent material. Water 'concentrates' prepared for *Cryptosporidium* and *Giardia* analysis contain numerous autofluorescent components with emission that spans the visible spectrum and thus limits the utility of spectral filtering techniques. As a demonstration of the power of temporal filtering, three different colored fluorescent polymer microspheres were obtained from Cospheric (Santa Barbara, CA); red (FMR-1UM-5UM), green (FMG-1UM-5UM), and yellow (FMY-1UM-5UM). These microspheres are intensely fluorescent and range in size from 1 to 5 μm; they were combined in approximately equal proportions to form a slurry in FEB. As a target for detection by the GALD, the bead mixture was spiked with a very dilute solution of luminescent europium polymer microspheres (Fluorospheres, 1 μm, F2088-2; Molecular Probes, Invitrogen Australia, P/L, Mt. Waverly, VIC, Australia). The mixture was then examined using sequentially, a CY3 filter set, a FITC filter set, and TGL analysis using the GALD.

RESULTS AND DISCUSSION

Epifluorescence Microscopy. The GALD housing was designed to permit the device to fit into the DIC slot on the nosepiece of a BX51 fluorescence microscope. This slot has dimensions 30 mm wide and 13 mm high to accommodate the

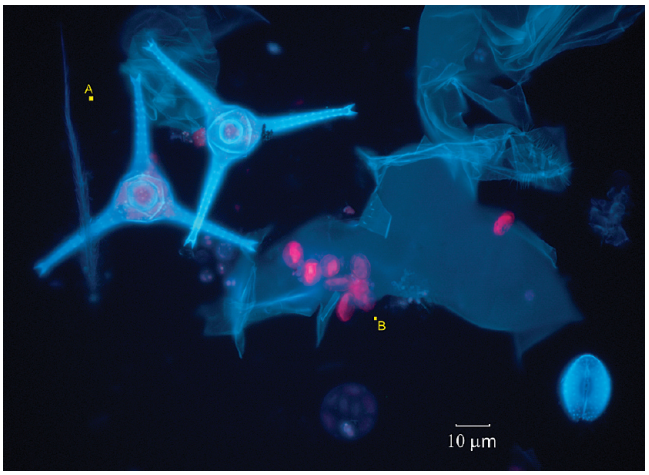

Figure 4. A photomicrograph (40×/0.75 dry objective) of sediment isolated from the community water supply by flocculation of 10 L of water. The image was captured on a 12.8 megapixel DP72 color camera (4140 × 3096) with an exposure of 18 s. *Giardia lamblia* cysts were labeled with a europium chelate prior to inoculation of the sediment; they fluoresce a bright red when excited in the UV. Excitation was by means of the filter-cube mounted UV LED that emits at 365 nm with a spectral spread of 10 nm. The three-armed desmids fluorescing sapphire-blue are a species of *Staurastrum*. For the purpose of comparing the relative signal-to-noise ratio (SNR) of epifluorescence and GALD images, a line-profile of pixel intensities was plotted for the pixels between the two points marked 'A' and 'B' and is shown as an insert in Figure 5.

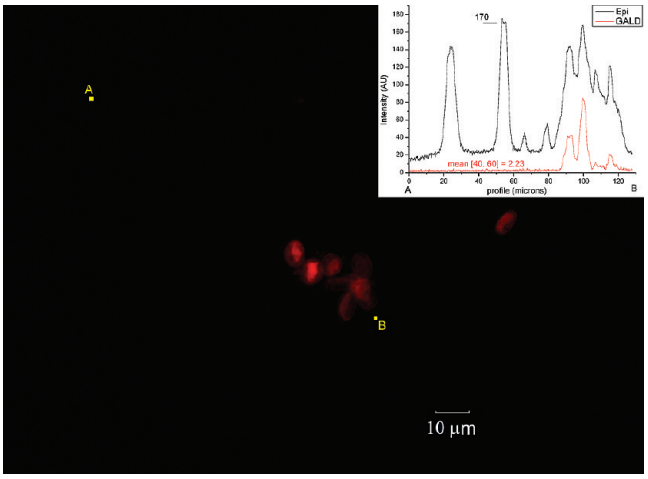

Figure 5. The sample view was identical to that seen in Figure 4 except that it was captured with the GALD in operation. *Giardia* cysts labeled with a europium chelate are now captured in the absence of autofluorescence using the same camera exposure. The two points used to mark the interval probed to generate the line profile are shown as 'A' and 'B'. Insert: The interval between the points marked 'A' and 'B' in Figures 4 and 5 were analyzed to compare pixel intensities. In epifluorescence mode, the arm of one of the desmids recorded a peak intensity of 170 (8-bit scale, max. = 255). With the GALD in operation, the autofluorescence background was reduced 76-fold, to an average of 2.33. Overall, the *Giardia* cysts recorded pixel intensities of about half that observed in epifluorescence mode.

DIC prism slider. In use, the slider is replaced with the GALD unit, the rotor blades of which can be locked (electronically) in an open position so that conventional bright-field or fluorescence microscopy can be employed or the instrument can be instantly switched to TGL mode.

With the GALD in operation, bright TGL images of labeled cysts were obtained. The improved visibility was due in part to the GALD design that replaces the dichroic with the highly reflective face of the rotor to ensure efficient transmission of the excitation beam to the sample. Previously, we reported the design of a UV LED excited TGL microscope[25] that employed a UV LED mounted within the filter-cube where the excitation filter would normally be situated. A UV sensitive phototransistor (Epigap, EPD-365−0/1.4) was mounted on a stainless steel "slide" to measure the excitation pulse energy of the filter cube mounted device relative to the GALD. Measurements were taken using a 40×/0.75 dry objective with both LEDs pulsed at 900 mA (independent tests). The GALD pulse was 7.2 fold more intense than the pulse delivered by the filter-cube mounted configuration described previously[25] (see Supporting Information).

Together with the improved excitation efficiency, the optical pathway in a GALD-equipped microscope is enhanced compared with a conventional TGL microscope because the delayed luminescence is not constrained to pass through the dichroic and suffer reflection losses. These advantages tend to compensate for the longer transition period imposed by the GALD. The europium chelate used for this work has a luminescence lifetime of around 640 μs, and because the decay follows single exponential decay kinetics it is possible to estimate the emission intensity (I_t) after a gate delay of 260 μs: $I_t = I_0 e^{-t/\tau}$; $I_t = I_0 e^{-260/640} = 0.66 I_0$

Thus, 66% of the initial intensity of the sample is available for detection after excitation has ceased and the aperture has fully opened. The excitation duty cycle of the GALD is 32% with a cycle time between pulses of 1.62 ms.

GALD Imaging of *Giardia* Cysts. *Giardia lamblia* is a waterborne protozoan parasite that can present a serious health risk to the very young or old or those with compromised immune systems. *Giardia* infection can occur through ingestion of active organisms (trophozoites) or dormant cysts: oval shaped, translucent organisms 8−15 μm in length. Detection of *Giardia* and other parasites in community water supplies using fluorescence microscopy is difficult because of the highly autofluorescent nature of the debris collected when sampling large volumes of water (10−100 L). The 'muddy' isolate contains numerous varieties of algae and desmids that autofluoresce strongly across a broad range of excitation wavelengths. For this report, the filtrate from a water sample was inoculated with *Giardia lamblia* cysts that had previously been labeled with a europium chelate. The images shown in Figures 4 and 5 were captured on an Olympus BX51 fluorescence microscope using a UPLANFI 40 X/0.75 (dry) objective. The image in Figure 4 was captured in conventional epifluorescence mode using the UV LED mounted in the filter-cube housing as previously described. Figure 5 shows time-gated luminescence as revealed by the GALD; both images were captured with identical camera settings and exposure of 18 s.

A line profile between the points marked 'A' and 'B' in Figures 4 and 5 was constructed to compare the luminous intensity of the labeled cysts versus the autofluorescence from the (three-armed) desmids (*Staurastrum*) in both images; the line profiles extracted are presented as an insert in Figure 5. Background autofluorescence is absent in Figure 5 with the GALD active; the profile extracted from this figure indicates luminous intensity of the cysts is reduced to half of that observed in epifluorescence mode (84/167). It is important to note, however, that autofluorescence was

dx.doi.org/10.1021/ac200281h |*Anal. Chem.* 2011, 83, 4782–4787

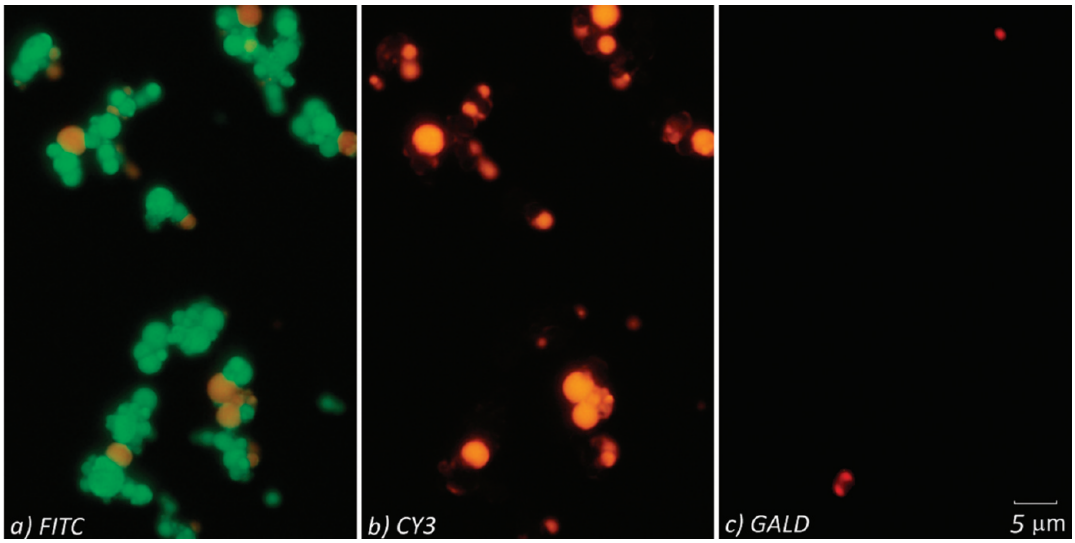

Figure 6. Intensely fluorescent 1−5 μm red, green, and yellow polymer spheres were mixed with 1 μm europium polymer spheres for TGL analysis. Each frame corresponds to the same region but was captured with a different filter set: frame A was captured with blue excitation from a FITC filter set, frame B was captured with green excitation from CY3 filter set and frame C was captured with the GALD in operation and no filter set. An exposure interval of 4 ms was used to capture frames A and B, and 600 ms for frame C. Images were captured on a BX51 Olympus microscope fitted with a 60× dry objective and DP72 camera with settings of 200 ASA, 24 bit color, image size of 1360 × 1024.

suppressed by a factor of 76 as evidenced by the relative intensities of the two plots at a common point (x = 54; 170/2.23). The signal (x = 100) to noise (x = 54) ratio for the image in Figure 4 is 0.98 (168/170) whereas for Figure 5 it is 37 (83/2.23), a significant improvement. Autofluorescence was completely suppressed, yet labeled cysts were clearly visible to the naked eye when the GALD was in operation.

Muliparameter Imaging. TGL detection schemes that utilize the more common europium and terbium chelates (τ > 100 μs) are ideal for use with the GALD described here. Delayed luminescence can be easily seen with the naked eye and captured with minimal exposure periods on a CCD camera. Liquid light guides can be employed to conveniently couple high intensity UV light into the device. This has the advantage that broad spectrum UV (320−370 nm) can be used for the excitation of multiple luminophores simultaneously. Terbium chelates typically require excitation around 340 nm, a wavelength that is beyond the capacity of current UV LEDs to deliver useful power. The ability to multiplex the detection of different targets is important for many assays. For example, probes containing distinct combinations of europium, terbium, and samarium ions have been used for seven-color time-resolved fluorescence hybridization assays.[26] However, we note that useful samarium chelates have relatively short luminescence lifetimes of 6−20 μs and are unlikely to display sufficient signal strength when viewed through the GALD. Other excellent examples of multiplexed detection are the mixed chelates of europium, terbium, palladium, and platinum for evaluation of peripheral blood leukocytes.[16,27,28] Palladium and platinum have shorter fluorescence lifetimes ($\tau_{max} \sim 91\,\mu$s) than europium chelates, and oxygen must be excluded to obtain optimum quantum yields. The GALD rotor speed must be increased to rotation speeds of 60 000 rpm or higher to provide sufficient signal intensity for these luminophores, a velocity beyond the range of our prototype device.

Temporal Gating To Suppress Microsphere Fluorescence. The *Cospheric* beads visible in frames a and b of Figure 6 have a broad excitation range although they are optimally excited by short wavelengths (365 nm). The green beads visible in Figure 6a were excited using a FITC filter set with excitation in the blue (490 nm) and selectively detected by the green barrier filter in the FITC filter cube; consequently, the red *Cospheric* beads are not visible in this frame. Figure 6b on the other hand was captured with the microscope equipped with the CY3 filter set (Ex: 510−560 nm, Em: 575−640 nm) that revealed in greater intensity the red and orange microspheres but suppressed emission from the green microspheres . The europium microspheres are not visible in either Figure 6a or 6b because they are optimally excited at 365 nm. Figure 6c was captured without the aid of a filter cube because it is unnecessary when the GALD is in operation. The exposure interval required to produce the image in Figure 6c was 150-fold longer (600 ms versus 4 ms) than that required for Figure 6a and 6b. The intense fluorescence from the Cospheric beads spanned the visible spectrum but was completely suppressed through temporal gating with the GALD.

High Speed TGL Imaging. it was possible to capture high contrast, well-defined images with the GALD using a short exposure of 100 ms when the microscope was fitted with the iXON camera. Frames captured in this mode delivered a SNR of 217/1.9 = 114:1. See Supporting Information for a full report on high speed GALD imaging and comparisons with other methods.

Imaging Artifacts and Target Resolution. The GALD rotor is a modified form of a chopper wheel that satisfies the dual requirements of switching the excitation beam and blocking the detection pathway. The conical surface of the GALD rotor serves only to reflect the incident excitation beam; it is removed from the optical pathway during the detection phase so that no image distortion occurs. Nevertheless, the rapidly spinning rotor has the potential to act as a source of vibration. The GALD was fabricated at the university workshop, and no attempt was made to balance the rotor wheel prior to assembly of the GALD. Furthermore, vibration-absorbing polymer fittings were not present on the device or within the microscope mounting cavity. Consequently, some vibration was present during operation of

the device, and this was minimized by insertion of a small piece of silicone tubing over the top of the grub screw used to lock the device in position. Suppression was adequate to ensure no blurring of the target image occurred.

In the detection phase, the GALD is out of the optical circuit and thus image resolution is a function of the microscope optics. The 1 μm beads share similar dimensions with bacteria yet are adequately resolved by the system as can be seen in Figure 6c

Retrofitting. Importantly, a readily available research microscope (Olympus BX51) can be converted to operate in TGL mode in less than 1 min by insertion of the GALD. Because the dichroic filter cube is not required for delayed luminescence imaging, it is conceivable that a simple, low cost microscope supporting bright-field imaging could operate in TGL mode if the GALD can be inserted into the optical path. The rotor can be locked in the open position (by briefly energizing the drive coils) so that other modalities are unaffected by its insertion. Longevity of the rotor bearings has not yet been determined, but two prototype devices have been in regular use for two years without problems.

CONCLUSION

Time-gated luminescence detection schemes have conventionally rested upon the paradigm that excitation and detection mechanisms are autonomous processes to be linked externally. In this report, I have described a simple device that autosynchronously aligns these two key states. Further, the ability of the device to permit the passage of only delayed luminescence opens the possibility of extended exposures on low-cost cameras for the sensitive capture of faint luminescence. In the study reported here, the intensity of the delayed luminescence was sufficient to permit rapid acquisition on the iXON camera, clear images being obtained in 100 ms. The current aim is to develop a TGL workstation equipped with the GALD/iXON camera to scan a slide more effectively than a human operator and process images on-the-fly. The simple design and small size of the GALD makes it possible to use the device for hand-held macroinspections of delayed luminescence, and this novel application is likely to prove fruitful. The UV LED was observed to be suitable for exciting luminescence from at least one terbium chelate: DTPA-cs124-NCS reported by Krasnoperov,[29] although laser excitation at 355 nm would deliver much brighter emission.

The GALD used for this work was an experimental device, but both the mirror finish on the rotor and the beam optics would benefit from further optimization. Nevertheless, europium chelates provided useful, high-brightness images with the GALD while prompt fluorescence was greatly suppressed.

ASSOCIATED CONTENT

Supporting Information. Additional information as noted in the text. This material is available free of charge via the Internet at http://pubs.acs.org.

AUTHOR INFORMATION

Corresponding Author
*E-mail: russell.connally@mq.edu.au.

ACKNOWLEDGMENT

Sincere thanks to the Macquarie Engineering and Technical Services (METS) division, particularly John Funnel and Walther Adendorff who deserve much praise for their diligent and careful workmanship in crafting numerous GALD prototypes. I also acknowledge and thank Richard Mildren for his valuable advice and suggestions regarding the manuscript and Noosha Ehya for her efforts in preparing the BHHCT-labeled *Giardia* cysts.

REFERENCES

(1) Lakowicz, J. R. *Principles of Fluorescence Spectroscopy*; Plenum Press: New York, NY, 1983.
(2) Lindquist, H. D.; Bennett, J. W.; Hester, J. D.; Ware, M. W.; Dubey, J. P.; Everson, W. V. *J. Parasitol.* **2003**, *89*, 865.
(3) Mounteer, A. H.; Passos, F. M. L.; Borges, A. C.; Silva, D. O. *Can. J. Microbiol.* **2002**, *48*, 245.
(4) Staughton, T. J.; McGillicuddy, C. J.; Weinberg, P. D. *J. Microsc.* **2001**, *201*, 70.
(5) Hongmanee, P.; Stender, H.; Rasmussen, O. F. *J. Clin. Microbiol.* **2001**, *39*, 1032.
(6) St Amand, A. L.; Frank, D. N.; De Groote, M. A.; Basaraba, R. J.; Orme, I. M.; Pace, N. R. *J. Clin. Microbiol.* **2005**, *43*, 5369.
(7) Beverloo, H. B.; van Schadewijk, A.; van Gelderen-Boele, S.; Tanke, H. J. *Cytometry* **1990**, *11*, 784.
(8) Marriott, G.; Clegg, R. M.; Arndt-Jovin, D. J.; Jovin, T. M. *Biophys. J.* **1991**, *60*, 1374.
(9) Beverloo, H. B.; van Schadewijk, A.; Bonnet, J.; van der Geest, R.; Runia, R.; Verwoerd, N. P.; Vrolijk, J.; Ploem, J. S.; Tanke, H. J. *Cytometry* **1992**, *13*, 561.
(10) Seveus, L.; Vaisala, M.; Syrjanen, S.; Sandberg, M.; Kuusisto, A.; Harju, R.; Salo, J.; Hemmila, I.; Kojola, H.; Soini, E. *Cytometry* **1992**, *13*, 329.
(11) Phimphivong, S.; Kolchens, S.; Edmiston, P. L.; Saavedra, S. S. *Anal. Chim. Acta* **1995**, *307*, 403.
(12) Phimphivong, S.; Saavedra, S. S. *Bioconjugate Chem.* **1998**, *9*, 350.
(13) Vereb, G.; Jares-Erijman, E.; Selvin, P. R.; Jovin, M. T. *Biophys. J.* **1998**, *74*, 2210.
(14) de Haas, R. R.; van Gijlswijk, R. P.; van der Tol, E. B.; Veuskens, J.; van Gijssel, H. E.; Tijdens, R. B.; Bonnet, J.; Verwoerd, N. P.; Tanke, H. J. *J. Histochem. Cytochem.* **1999**, *47*, 183.
(15) Tanke, H. J.; De Haas, R. R.; Sagner, G.; Ganser, M.; Van Gijlswijk, R. P. M. *Cytometry* **1998**, *33*, 453.
(16) Soini, A. E.; Kuusisto, A.; Meltola, N. J.; Soini, E.; Seveus, L. *Microsc. Res. Tech.* **2003**, *62*, 396.
(17) Connally, R., E; Veal, D., A; Piper, J. *Cytometry, Part A* **2006**, *69A*, 1020.
(18) Connally, R.; Piper, J. *J. Biomed. Opt.* **2008**, *13*, 034022.
(19) Buenzli, J.-C. G. *Chem. Rev. (Washington, DC, U.S.)* **2010**, *110*, 2729.
(20) Bunzli, J.-C. G. *Chem. Lett.* **2009**, *38*, 104.
(21) Bunzli Jean-Claude, G.; Piguet, C. *Chem. Soc. Rev.* **2005**, *34*, 1048.
(22) Eliseeva, S. V.; Bunzli, J.-C. G. *Chem. Soc. Rev.* **2010**, *39*, 189.
(23) Yuan, J.; Matsumoto, K. *Anal. Chem.* **1998**, *70*, 596.
(24) Arnaud, N.; Georges, J. *Analyst* **1997**, *122*, 143.
(25) Connally, R. E.; Veal, D. A.; Piper, J. *Cytometry: Part A* **2006**, *69A*, 1020.
(26) Samiotaki, M.; Kwiatkowski, M.; Ylitalo, N.; Landegren, U. *Anal. Biochem.* **1997**, *253*, 156.
(27) Hennink, R. J.; de Haas, R.; Verwoerd, N. P.; Tanke, H. J. *Cytometry* **1996**, *24*, 312.
(28) de Haas, R.; van Gijlswijk, R. P. M.; van der Tol, E. B.; Zijlmans, H. J. M. A. A.; Bakker-Schut, T.; Bonnet, J.; Verwoerd, N. P.; Tanke, H. J. *J. Histochem. Cytochem.* **1997**, *45*, 1279.
(29) Krasnoperov, L. N.; Marras, S. A. E.; Kozlov, M.; Wirpsza, L.; Mustaev, A. *Bioconjugate Chem.* **2010**, *21*, 319.
(30) Marriott, G.; Heidecker, M.; Diamandis, E. P.; Yan-Marriott, Y. *Biophys. J.* **1994**, *67*, 957.